ELSEVIER

Journal of Fluids and Structures 20 (2005) 567–575

JOURNAL OF FLUIDS AND STRUCTURES

www.elsevier.com/locate/jfs

Detailed flow and force measurements in a rotated triangular tube bundle subjected to two-phase cross-flow

M.J. Pettigrew*, C. Zhang, N.W. Mureithi, D. Pamfil

BWC/AECL/NSERC Chair of Fluid–Structure Interaction, Department of Mechanical Engineering, École Polytechnique Montréal, Que., Canada H3T 1J4

Received 20 September 2004; accepted 19 February 2005
Available online 10 May 2005

Abstract

Two-phase cross-flow exists in many shell-and-tube heat exchangers. A detailed knowledge of the characteristics of two-phase cross-flow in tube bundles is required to understand and formulate flow-induced vibration parameters such as damping, fluidelastic instability, and random excitation due to turbulence. An experimental program was undertaken with a rotated-triangular array of cylinders subjected to air/water flow to simulate two-phase mixtures. The array is made of relatively large diameter cylinders (38 mm) to allow for detailed two-phase flow measurements between cylinders. Fiber-optic probes were developed to measure local void fraction. Local flow velocities and bubble diameters or characteristic lengths of the two-phase mixture are obtained by using double probes. Both the dynamic lift and drag forces were measured with a strain gauge instrumented cylinder.

1. Introduction

Two-phase cross-flow exists in many shell-and-tube heat exchangers, for instance, in the U-tube region of nuclear steam generators. A detailed knowledge of the characteristics of two-phase cross-flow in tube bundles is required to understand and formulate flow-induced vibration parameters such as damping, hydrodynamic mass, fluidelastic instability, and random excitation due to turbulence. The information is also required to validate tube-scale thermal–hydraulic analyses and to understand local crud deposition mechanisms.

Prior to 1980, very little work had been done to study flow-induced vibration of tube bundles subjected to two-phase cross-flow. Since then a few studies were conducted in this area. This work was reviewed by Pettigrew and Taylor (1994). Since 1994, several researchers have contributed relevant results, in particular, Feenstra et al. (1995, 2002) in Freon 11 two-phase flow, Mann and Mayinger (1995) in Freon 12 two-phase flow, and Nakamura et al. (2002), Mureithi et al. (2002) and Hirota et al. (2002) in steam–water cross-flow. Also, comprehensive studies on vibration of tube bundles subjected to both air–water and Freon 22 two-phase cross-flow were conducted at the Chalk River Laboratories (Pettigrew et al., 2001, 2002). To our knowledge, no detailed measurements of two-phase flow in tube arrays have ever been done.

An experimental program was undertaken with a rotated-triangular array of cylinders subjected to air/water flow to simulate two-phase mixtures. The array, which has a pitch-to-diameter ratio of 1.5, is made of relatively large diameter

*Corresponding author.
E-mail address: michel.pettigrew@polymtl.ca (M.J. Pettigrew).

0889-9746/$ - see front matter
doi:10.1016/j.jfluidstructs.2005.02.007

cylinders (38 mm). This results in larger gaps (19 mm) between cylinders to allow for detailed two-phase flow measurements.

Fiber-optic probes were developed to measure local void fraction. Local flow velocities and bubble diameters or characteristic lengths of the two-phase mixture are also obtained by using double probes. Both the dynamic lift and drag forces were measured with a strain gauge instrumented cylinder. The results of these detailed two-phase flow and force measurements are presented in this paper. An attempt is made to use this information to understand vibration excitation mechanisms in two-phase cross-flow.

2. Experimental considerations

2.1. Test loop

The experiments were done in an air–water loop to simulate two-phase flows. The loop comprised a 25 l/s variable speed pump, a magnetic flow meter, a 2500 l tank, a 250 l/s compressed air supply system and connecting piping as shown in Fig. 1.

The compressed air was injected below a suitably designed mixer to homogenize and distribute the two-phase mixture uniformly below the test-section. The air flow was measured with orifice plates connected to a differential pressure transducer and electronic readout system. The loop was operated at room temperature and the pressure in the test-section was slightly above atmospheric.

2.2. Test-section

The test-section, which has an essentially rectangular cross-section ($99 \times 191\ \text{mm}^2$), is shown in Fig. 2. It consists of a column of six 38 mm diameter cylinders flanked on either side by half cylinders to simulate essentially the flow path in a large array of cylinders in a rotated triangular configuration.

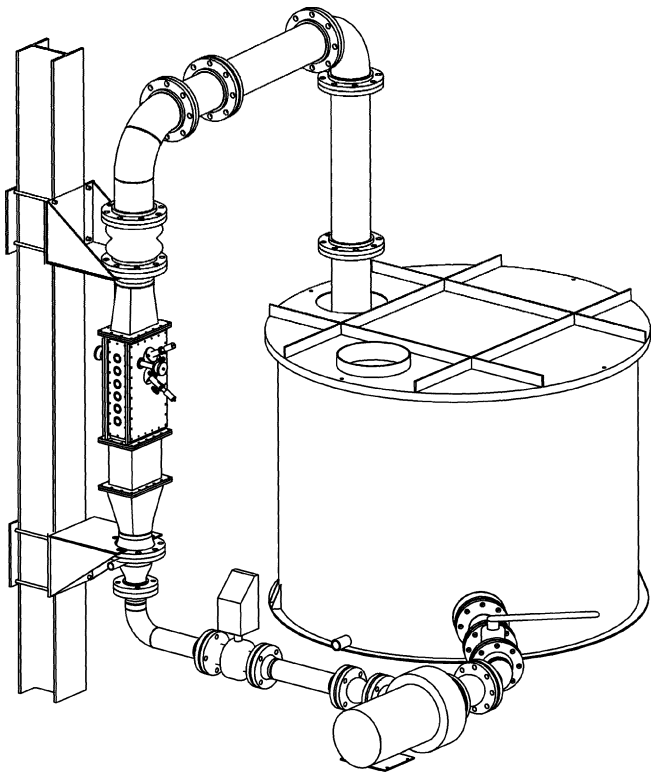

Fig. 1. Test loop.

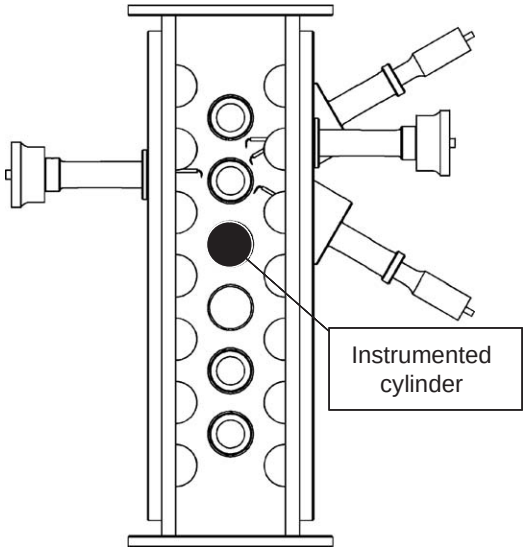

Fig. 2. Test-section.

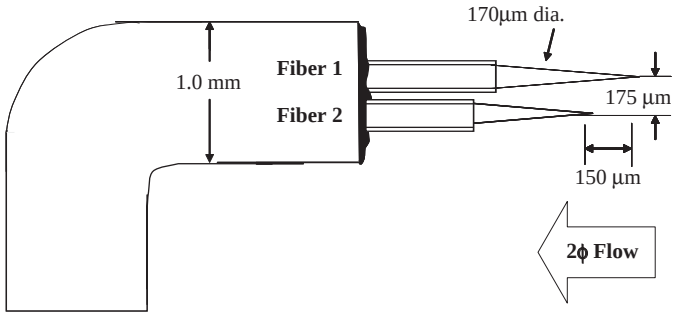

Fig. 3. Double fiber optic probe.

The pitch-to-diameter ratio, P/D, was 1.5 resulting in an inter-cylinder gap of 19 mm which allowed sufficient space for detailed flow measurements. The test-section length-to-gap width ratio is 10, thus, adequate to maintain essentially two-dimensional flow. The measurements were taken every millimeter with fiber-optic probes assembled within a traversing mechanism. The tip of the probes could be positioned accurately with a micrometer head.

The probe assemblies were installed at four principal positions in the array as shown in Fig. 2. These positions are henceforth called lower and upper 60° for the narrow gaps between cylinders and lower and upper 90° for the larger flow areas between upstream and downstream cylinders. One cylinder was instrumented with strain gauges to measure the dynamic drag and lift forces due to the two-phase flow.

2.3. *Fiber-optic probes for two-phase flow measurements*

Fig. 3 shows a double fiber-optic probe, which comprises two fiber-optic probes inserted in one stainless tube. Each probe has a conical tip and is made of an optical fiber of 170 μm diameter. It acts as a phase sensor based on the different level of light reflection between air and water. Two flow conditions were investigated in detail, i.e., 50 and 80% volumetric void fraction at a nominal pitch flow velocity, U_p, of 5 m/s.

For each measurement, the probe data were recorded for a period of 20 s at a 2×10^6 Hz sampling rate. A data analysis software was developed to obtain the time, T_i, at which the ith gaseous particle touches the probe, and the duration of this contact, τ_i, as schematically illustrated in Fig. 4. The void fraction can be obtained from either probe

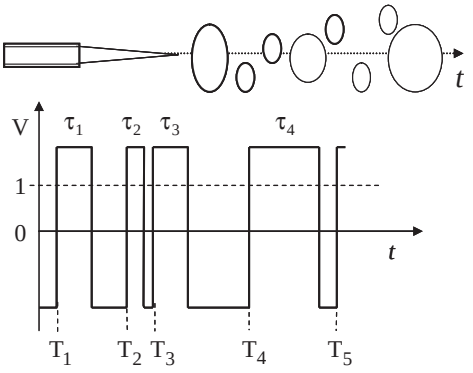

Fig. 4. Void fraction measurement.

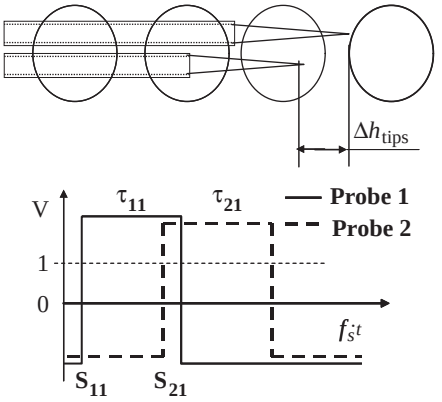

Fig. 5. Bubble velocity and bubble size measurements.

from the ratio of integrated gas-phase contact times, τ_i, over the total test time, T. It can be expressed as

$$\varepsilon(x,T)=\frac{1}{T}\sum_i \tau_i. \tag{1}$$

The bubble or gas phase velocity can be estimated from the transit time between the two tips, which are a known distance apart (around 150 μm), as shown in Fig. 5. It can be expressed as

$$V_i(x,t)=\frac{\Delta h_{\text{tips}}}{\Delta T_i}, \tag{2}$$

where

$$\Delta T_i=\frac{1}{f_s}(S_{2i}-S_{1i}), \tag{3}$$

where f_s is the sampling rate for the signal, and S_{1i}, S_{2i} are the sampling points when the ith bubble contacts the first probe and second probe, respectively.

The bubble size, d, can be deduced from the product of bubble velocity and contact duration. This is expressed as

$$d_{1i}=V(x,t)\tau_{1i} \quad \text{and} \quad d_{2i}=V(x,t)\tau_{2i} \tag{4}$$

for probe 1 and 2, respectively.

In this study, the bubble velocity is the average value of the velocities of analyzed bubbles. Analyzed bubbles are the bubbles that satisfy two criteria. One is that the calculated velocity has to be within a velocity range between 1 and 10 m/s (for the $U_p=5$ m/s case). The other is that the relative error of bubble sizes between the first probe and second probe, $(d_{1i}-d_{2i})/d_{1i}$, be less than 5%. The bubble size is the average of $V\tau_{1i}$ from the first probe.

2.4. Instrumentation

Both the dynamic lift and drag forces were measured with a strain gauge instrumented cylinder in the fourth position from the upstream end of the test-section (Fig. 2). The instrumented cylinder was cantilevered and surrounded by rigid tubes. Two pairs of diametrically opposite strain gauges were installed in the cylinder at 90° from each other to measure the forces in the flow direction (drag) and in the direction normal to the flow (lift). The strain gauges were connected to strain indicators. Before the instrumented cylinder was inserted into the test-section, the static strain–force relation was determined via a careful calibration. The signals were routinely analyzed on an OR38 8-32 channel real-time multi-analyzer/recorder coupled to a lap-top computer.

3. Results

3.1. Flow measurements

Typical detailed measurements along the lower 60° line across the narrowest gap between cylinders are shown in Fig. 6. Due to assembly problems, the probe tips were not exactly on the 60° and 90° lines. In fact the tips were roughly 2 mm downstream of the lines. Although this will be corrected in future tests, we do not believe this slight misalignment affected much the results. The measurements were taken every millimeter across the 19 mm gap. The measurements were remarkably stable as may be seen by the lack of scatter in the data. The measurements of void fraction, bubble velocity (gas-phase velocity) and bubble size (characteristic lengths of the two-phase mixture) are shown in Figs. 6(a)–(c), respectively. These measurements correspond to homogeneous flow conditions of 80% void fraction and gap flow velocity of 4.33 m/s (pitch velocity of 5 m/s). The average measured gap bubble velocity and void fraction are respectively, 4.55 m/s and 73%. This indicates nearly homogeneous two-phase flow conditions. The slip between the gas and liquid phase is small. The bubble sizes range from 0.5 to 5 mm.

The results for all the flow measurements are summarized in Fig. 7. It shows that the flow velocity is relatively uniform across the lower and upper 60° gaps between cylinders. The flow velocity distribution in the lower and upper 90° space between cylinders is much less uniform. There is also a region of low flow velocity immediately upstream and downstream of the cylinders. It also shows an abrupt increase in velocity at a position corresponding to a transition between a more stagnant region between tubes and the main stream of the flow. It appears from both these measurements and visual observation that the flow streams through the available flow path between cylinders. This flow path is outlined with dash lines in Fig. 7. The region of low flow and the transition are more pronounced in between the half-tubes near the wall of the test-section than in the centre of the test-section. This is not surprising, since the wake between cylinders in the centre of the test-section is quite unsteady due to the absence of a solid boundary.

The void fraction distribution in the narrow 60° gaps is nearly uniform for the 80% void fraction tests whereas it is much less uniform for the 50% tests (Fig. 7(b) versus (a)). Interestingly, the void fraction distribution for the lower 60° gap is the mirror image of that for the upper 60° gap. This is expected because of symmetry. The void fraction is generally lower in the more stagnant regions between cylinders.

The bubble size distribution in the narrow 60° gaps is very similar to the void fraction distributions in the same locations (Fig. 7(e) versus (a) and Fig. 7(f) versus (b)). This is reasonable because the bubble size should be consistent with the void fraction. The bubble size distribution in the lower and upper 90° space is essentially similar to the void fraction distributions in the same location except in the centre of the test-section for the upper 90° measurement (Fig. 7(e) versus (a) and Fig. 7(f) versus (b)). This requires further investigation.

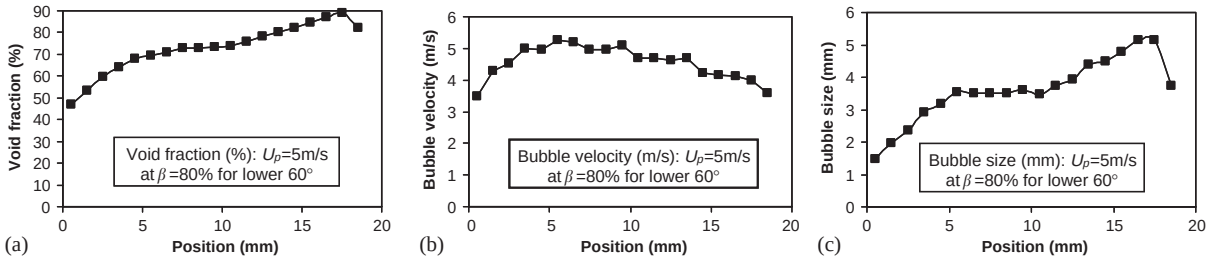

Fig. 6. Typical results of flow measurements: (a) void fraction; (b) bubble velocity; and (c) bubble size.

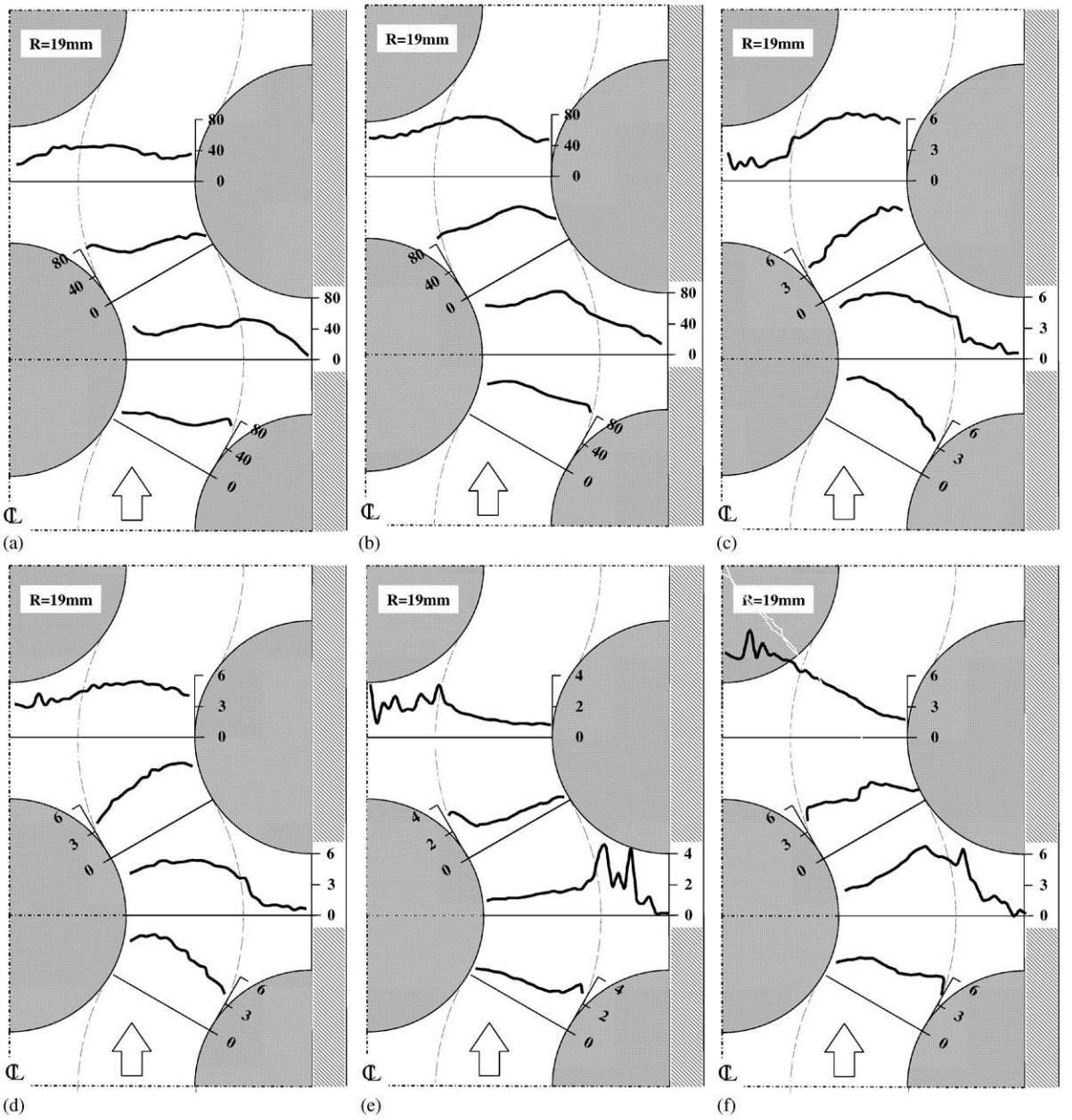

Fig. 7. Summary of results of flow measurements: void fraction (%) for $U_p = 5\,\mathrm{m/s}$ at (a) $\beta = 50\%$, (b) $\beta = 80\%$; bubble velocity (m/s) for $U_p = 5\,\mathrm{m/s}$ at (c) $\beta = 80\%$, (d) $\beta = 50\%$; bubble size (mm) for $U_p = 5\,\mathrm{m/s}$ at (e) $\beta = 50\%$ and (f) $\beta = 80\%$.

The bubble flow velocities and the corresponding measured void fraction in the lower and upper 60° gaps were integrated to obtain the total volumetric gas flow. The values are compared to the measured volumetric air flow at the inlet of the test-section in Table 1. The values are similar, thereby giving some degree of confidence in the measurement method.

3.2. Dynamic lift and drag force measurements

Force measurements were taken with an instrumented cylinder located in the fourth cylinder position from the upstream end of the test-section. Typical lift and drag force spectra are shown in Fig. 8. The spectra reveal narrow band

Table 1
Comparison between input and measured air flow rate

Probe	$\beta = 50\%$		$\beta = 80\%$	
	Input (l/s)	Measured (l/s)	Input (l/s)	Measured (l/s)
Upper 60°	15.7	14.64	25	23.67
Lower 60°	15.7	15.61	25	23.67

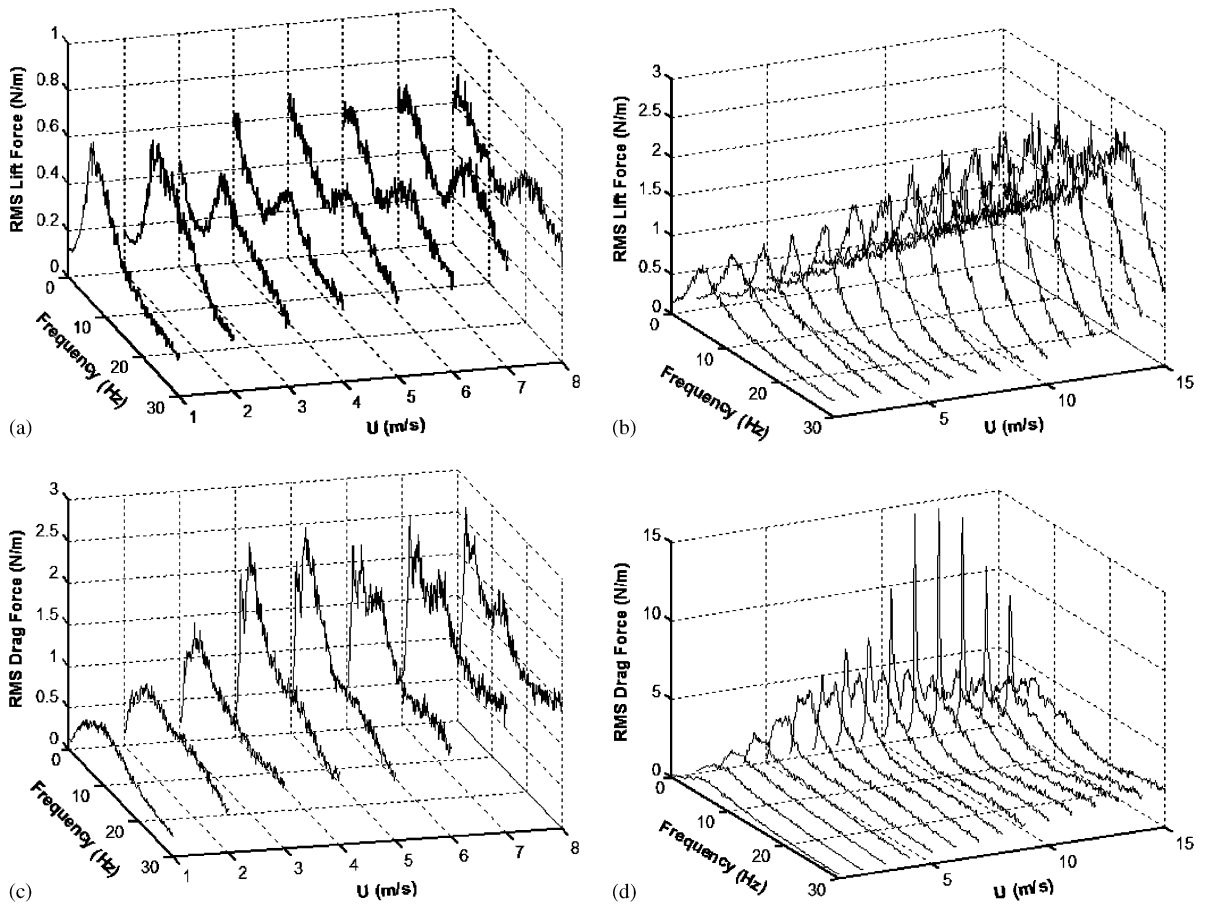

Fig. 8. Typical dynamic force spectra: (a) lift force spectra for (a) $\beta = 50\%$, (b) $\beta = 80\%$; drag force spectra for (c) $\beta = 50\%$ and (d) $\beta = 80\%$.

or quasi-periodic forces. This is somewhat unexpected and unlike typical random turbulence excitation. For the case of 80% void fraction, in the lift direction the periodic force frequency increases from about 5.75 to 21.75 Hz for a corresponding increase in flow velocity of 1–15 m/s (Fig. 9(b)). This yields Strouhal numbers from 0.22 to 0.06. Although periodic wake shedding was not expected at such high void fraction, the wake between cylinders was observed visually to be quite unsteady.

Periodicity was also observed in the drag direction as shown in Figs. 8(c) and (d). Surprisingly, for the case of 80% void fraction, the frequency of the periodic drag forces decreases slightly from 6.6 to 3.0 Hz at 6 m/s flow velocity and then increases slightly from 3.0 to 6.6 Hz for an increase in flow velocity from 6 to 15 m/s. The resulting drag forces increase with flow velocity from 1 to 8 m/s and then decrease slightly above 8 m/s flow velocity. They reach a maximum of roughly 6 N/m r.m.s. at 8 m/s flow velocity which is not insignificant. This behavior is still in search of an

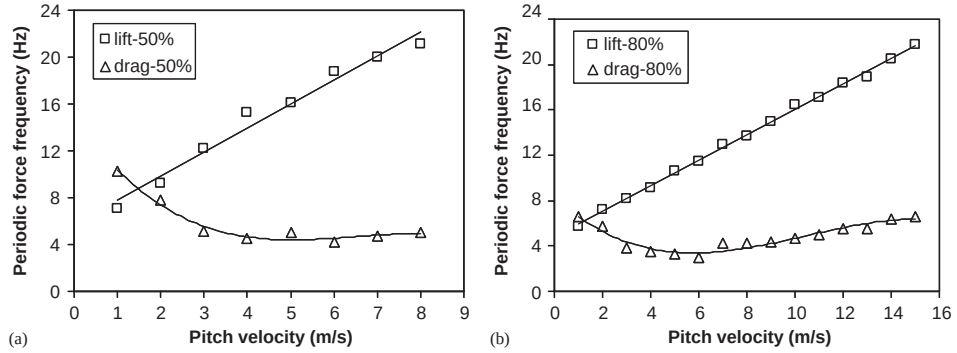

Fig. 9. Relationship between periodic force frequency and pitch velocity: (a) $\beta = 50\%$ and (b) $\beta = 80\%$.

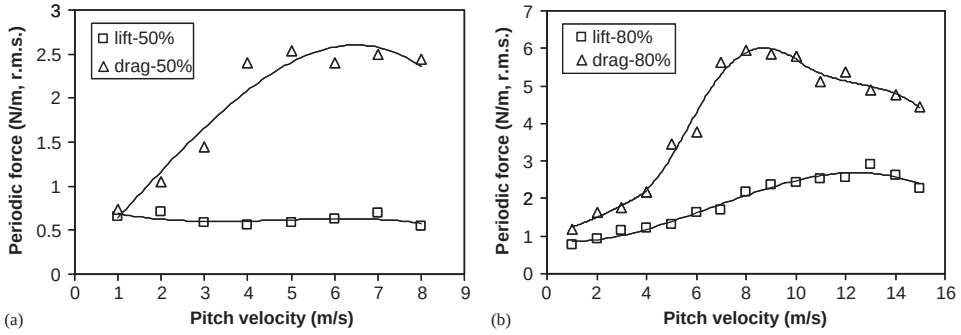

Fig. 10. Relationship between r.m.s. periodic force and pitch velocity: (a) $\beta = 50\%$ and (b) $\beta = 80\%$.

explanation. It is probably related to two-phase flow patterns. Some very sharp peaks at low frequency (around 2 Hz) also appeared at high mass fluxes as shown in Figs. 8(c) and (d). They are probably due to low-frequency loop oscillations.

The same results presented in terms of the relation between frequency and pitch velocity, and the relation between r.m.s. periodic force and pitch velocity may be found in Figs. 9 and 10.

4. Discussion

The results of flow measurement indicate that the flow tends to stream between the cylinders and that within that stream the flow velocity is fairly uniform. In fact, the flow path resembles a series of two-dimensional 60° elbows. Thus, it is not surprising that the void fraction distribution is not uniform. The lowest void fraction corresponds to the extrados and the highest void fraction to the intrados at the exit of the elbows (Figs. 7(a)–(c)) as would be expected of two-phase flow in elbows. The void fraction distribution has to completely reverse from one side to the other within half a cylinder pitch. That implies considerable mixing at each half-pitch interval. Thus, it is not surprising that the two-phase mixture is fairly homogeneous and the slip between phases is small.

The results of force measurement indicate that unexpected quasi-periodic forces were measured in both the drag and lift direction. These forces are significantly larger in the drag direction.

5. Conclusions

Detailed flow and force measurements were taken in a rotated triangular array of cylinders subjected to two-phase cross-flow. The results show that the two-phase flow tends to stream between the cylinders and that, within that stream,

the flow velocity is fairly uniform. The two-phase flow within the stream is fairly homogeneous, and the slip between phases appears to be relatively small. Unexpected quasi-periodic forces were measured in both the drag and lift direction.

References

Feenstra, P.A., Judd, R.L., Weaver, D.S., 1995. Fluidelastic instability of a tube array subjected to two-phase R-11 cross-flow. Journal of Fluids and Structures 9, 747–771.

Feenstra, P.A., Weaver, D.S., Judd, R.L., 2002. Modelling two-phase flow-excited damping and fluidelastic instability in tube arrays. Journal of Fluids and Structures 16, 811–840.

Hirota, K., Nakamura, T., Kasahara, J., Mureithi, N.W., Kusakabe, T., Takamatsu, H., 2002. Dynamics of an in-line tube array subjected to steam–water cross-Flow, Part III: fluidelastic instability tests and comparison with theory. Journal of Fluids and Structures 16, 153–173.

Mann, W. and Mayinger, F., 1995. Flow-induced vibration of tube bundles subjected to single- and two-phase cross-flow. Proceedings of the Second International Conference on Multiphase Flow, vol. 4, Kyoto, Japan, pp. 9–15.

Mureithi, N.W., Nakamura, T., Hirota, K., Murata, M., Utsumi, S., Kusakabe, T., Takamatsu, H., 2002. Dynamics of an in-line tube array subjected to steam–water cross-flow, Part II: unsteady fluid forces. Journal of Fluids and Structures 16, 137–152.

Nakamura, T., Hirota, K., Watanabe, Y., Mureithi, N.W., Kusakabe, T., Takamatsu, H., 2002. Dynamics of an in-line tube array subjected to steam–water cross-flow, Part I: two-phase damping and added mass. Journal of Fluids and Structures 16, 123–136.

Pettigrew, M.J., Taylor, C.E., 1994. Two-phase flow induced vibration: an overview. ASME Journal of Pressure Vessel Technology 116, 233–253.

Pettigrew, M.J., Taylor, C.E., Kim, B.S., 2001. The effects of tube bundle geometry on vibration in two-phase cross flow. Special FSI Issue of ASME Journal of Pressure Vessel Technology 123, 414–420.

Pettigrew, M.J., Taylor, C.E., Janzen, V.P., Whan, T., 2002. Vibration behavior of rotated triangular tube bundles in two-phase cross flows. ASME Journal of Pressure Vessel Technology 124, 144–153.